

Direct phase measurement interferometer working at 3.8 μm

K. N. Prettyjohns, S. DeVore, Eustace Dereniak, and James C. Wyant

A direct phase measurement interferometer designed and constructed to operate at a 3.8- μm wavelength is described. The interferometer uses a deuterium fluoride laser as the light source, zinc selenide transmitting optics, and a 32- X 64-element PtSi infrared CCD detector array with digital processing electronics and a graphics display on a desktop microcomputer. The instrument, which is useful for measuring a figure error caused by thickness variations in dielectric coatings applied to infrared optics, gives a wave front measurement repeatability of $<\lambda/50$ rms.

I. Introduction

It is always best to test an optical system at the wavelength at which it is to be used. This is especially true for optical systems containing high-reflectivity multilayer dielectric coatings required for 3.8- μm high-power laser systems, since extremely small thickness nonuniformity in these multilayer dielectric coatings can introduce unacceptable wave front phase errors. Furthermore, since these wave front phase errors depend on the wavelength in a rather complicated manner, it is not practical to perform measurements in the visible and extrapolate the results to the IR wavelength at which the coatings are to be used.

For metallic coatings, wave front phase errors introduced by coating thickness nonuniformity are generally negligible because the coatings are thin, typically 1000-1500 \AA , and hence the physical thickness variations are small, even for a large percentage film nonuniformity. This is not the case for dielectric coatings. Dielectric coatings are thick, typically 4000-6000 \AA , or more for each layer of a multilayer dielectric (MLD) coating designed for a wavelength of 3.8 μm , and there are six to ten layers in a typical MLD stack. Thus a small thickness change in each layer may introduce a rather large equivalent figure error, i.e., a large wave front phase error.

Figure 1¹ illustrates a typical equivalent figure error introduced by nonuniform film thickness across a mirror for a multilayer high-reflectance dielectric coating. For this example, a design for a wavelength of 3.8 μm , a 4% error in the thickness causes a reflectance drop of only 0.00003. However, a 4% error in the thickness causes an equivalent figure error of 0.04 waves at a wavelength of 3.8 μm .

To measure this equivalent figure error, one is tempted to use an interferometer working at a visible wavelength since these interferometers are readily available and easy to use. However, two problems may arise when using a visible wavelength interferometer to evaluate coatings intended for use at IR wavelengths. First, a coating having a high reflectance in the IR may have a very low reflectance in the visible. Second, and perhaps more important, as shown in Fig. 2, there is not simply a wavelength scale factor between equivalent figure errors measured in the visible and equivalent figure errors measured in the IR. It is perhaps possible to make several measurements at different wavelengths in the visible and extrapolate these results to the IR, but such techniques are risky at best.² If at all possible, equivalent figure errors should be measured at the wavelength at which the coatings are to be used. For this reason, a 3.8- μm wavelength Twyman-Green interferometer using phase shifting techniques to measure the phase distribution across the wave front was designed.

II. Interferometer Design

The interferometer is of the Twyman-Green type as illustrated schematically in Fig. 3. A photograph of the interferometer is shown in Fig. 4. The 3.8- μm source is a Helios model CLIIIb DF laser. Except for the laser, the entire interferometer is built on a single aluminum plate. Alignment between the laser and interferometer

The authors are with University of Arizona, Optical Sciences Center, Tucson, Arizona 85721.

Received 5 January 1985.

0003-6935/85/142211-06\$02.00/0.

© 1985 Optical Society of America.

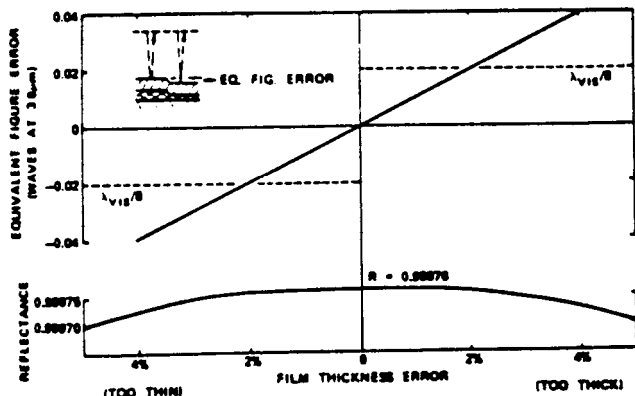


Fig. 1. Equivalent figure error in a MLD coated mirror. Air $|(HL)^4yH|Ag, H = \frac{1}{4}$ -wave ZnS, $L = \frac{1}{4}$ -wave ThF.¹

plate is accomplished by means of several beam-directing mirrors external to the interferometer. Single-frequency operation of the laser at 3.8 μm is achieved by using a grating as the output coupling. In this mode, 450 mW of power can be obtained at the laser output. If necessary, this power can be reduced through an output filter or by adjusting the laser controls.

Transmissive elements of the interferometer optics are made of ZnSe while reflective elements use enhanced aluminum broadband coatings. This choice of materials allows use of a He-Ne laser for interferometer alignment. The beam splitter is a ZnSe plate, AR coated on one surface. The uncoated surface acts as the beam splitter with a reflectance of -30%. The trans-

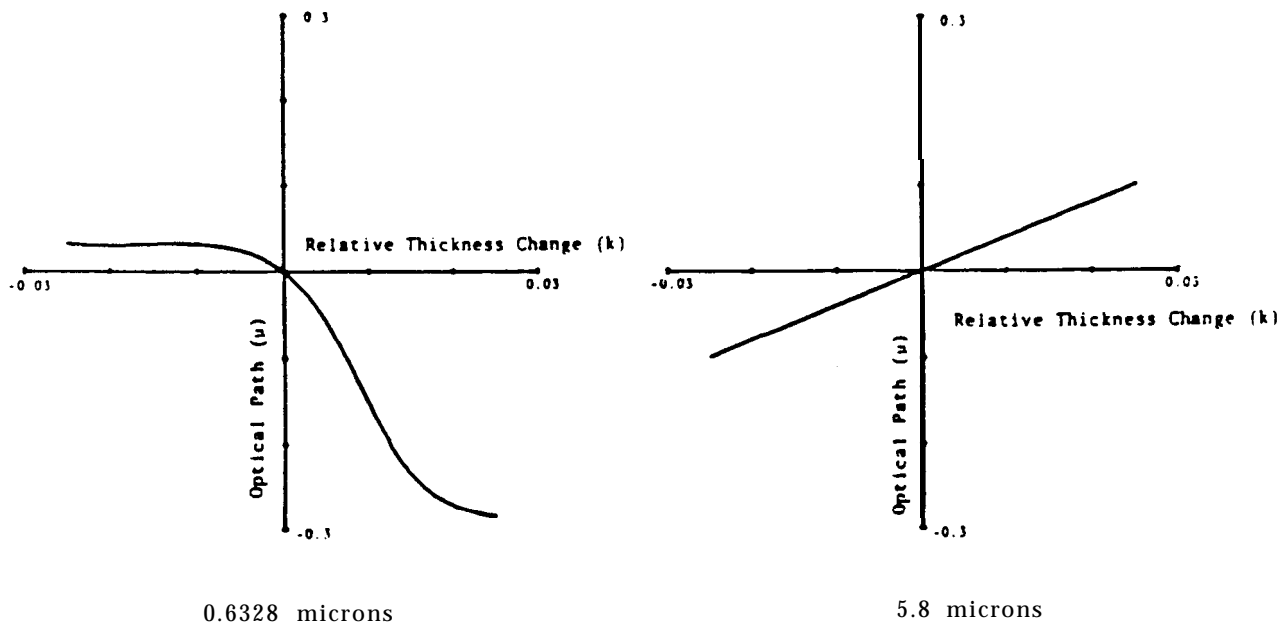


Fig. 2. Optical path change for a six-layer enhanced reflector as a function of thickness change. Design wavelength is 3.8 μm . Design reflectivity is 0.99919. Air $|(HL)^3HxL|Ag, H = \frac{1}{4}$ -wave ZnS, $L = \frac{1}{4}$ -wave ThF.²

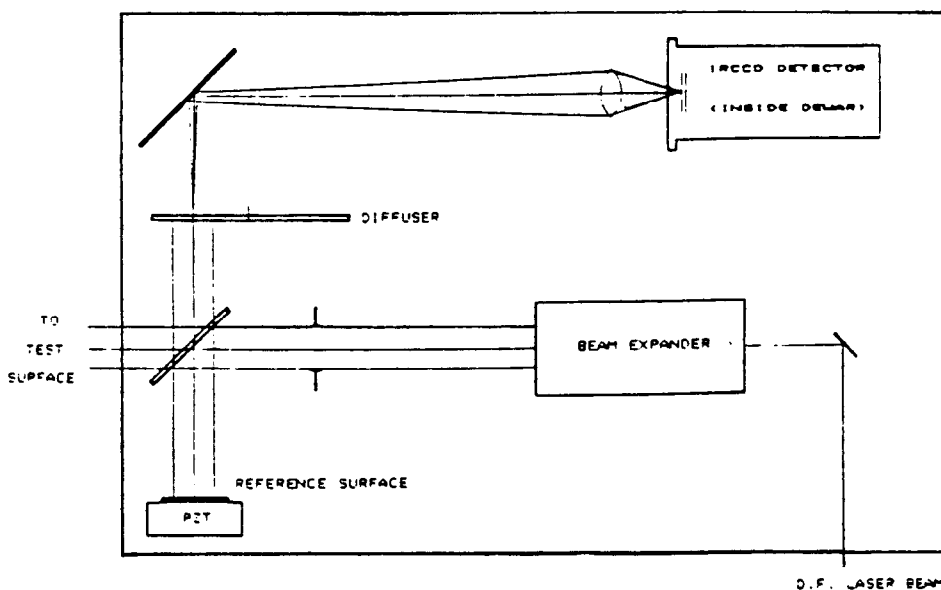


Fig. 3. Schematic of interferometer optical layout.

mitted test beam diameter is 22 mm. Additional optics expand this beam to the required diameter to test the high-power optics. The reference mirror is mounted on a piezoelectric transducer (PZT), which is controlled by the electronic interface described below.

The fringes are formed on a calcium fluoride diffuser and incoherently imaged onto the IRCCD array using a germanium lens operating at $f/2$. This latter step in the imaging optics was necessary to control unwanted fringes caused by internal reflections that would otherwise appear in the image formed on the IRCCD.

III. Infrared CCD Detector Array

The greatest difficulties were encountered with the detector and associated electronics of the interferometer. The detector chosen for imaging the interference pattern was an infrared charge-coupled device (IRCCD). To reconstruct a 2-D map of the wave front phase, it is necessary to sample the interference image in a 2-D grid of data points. Although this could be done using a pyroelectric vidicon tube,³ these suffer from image lag, are less rugged, and respond only to time-varying imagery. Research on IRCCDs with response in the 3-5- μm region has progressed⁴ over the past few years, and imagers of 64 X 128 elements are now available.⁵

The detector chosen for this instrument was the Honeywell 2793 IRCCD. This device is a 32 X 64 array of platinum-silicide Schottky photodiodes with an interline transfer CCD readout architecture as shown in Fig. 5. Our device was housed in a 40-pin DIL package with a rectangular hole in the back of the package (since the device is back illuminated in use). The 32 X 64 elements form a rectangular array, and the interference image is formed on the central 32 X 32 elements in our case. The array must be operated at -80 K and must, therefore, be housed in a liquid nitrogen Dewar.

Fixed pattern noise and pixel-to-pixel response variations can be severe problems when imaging with IRCCDs, and often special circuitry must be used to correct for these effects.⁶ However, as described below, the phase measurement algorithm provides a frame-to-frame subtraction (removing fixed pattern noise) and a frame-to-frame division (effectively normalizing response variations).

IV. CCD Drive and Data Acquisition System

The 2793 array requires nine different clocks and ten different dc bias voltage sources. These all must be adjusted to obtain the best device performance. Development of the optimal timing and dc bias levels was carried out using a universal CCD test facility.⁷ After determining the exact clock and dc drive requirements, a dedicated circuit was designed and constructed on a printed circuit card. This allowed operation at up to 500,000 pixels/sec, but because of other circuit limitations the best imagery was obtained at 250,000 pixels/sec. At this speed each video pixel is valid for $<2 \mu\text{sec}$ because of the presence of dummy pixels between the valid pixels as shown in Fig. 6. This effect is inherent in the device because of its architecture.

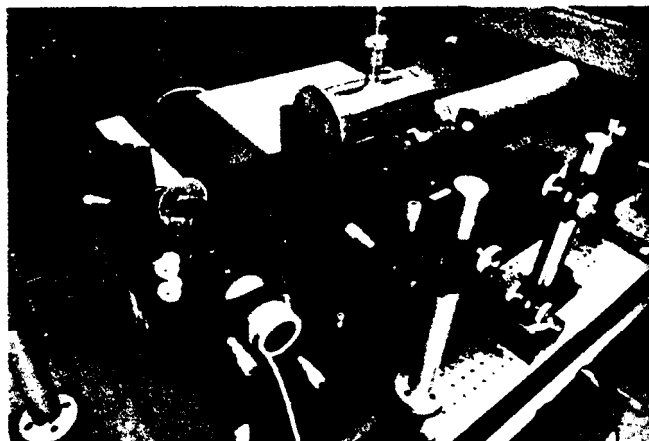


Fig. 4. Interferometer optical layout.

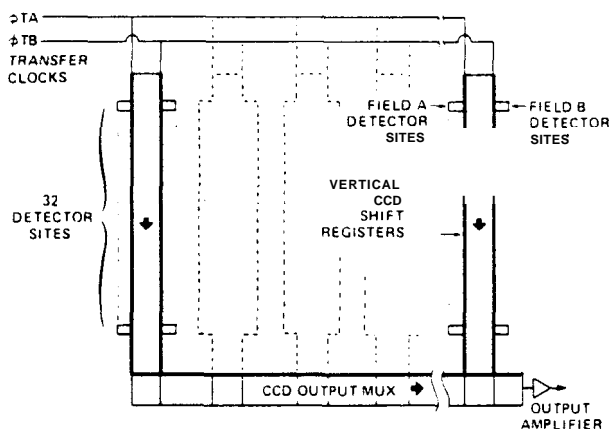


Fig. 5. Interlaced, interline transfer architecture of the Honeywell 2793 IRCCD.

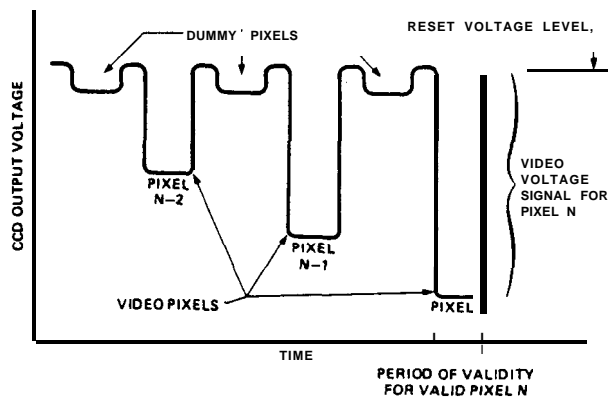


Fig. 6. Portion of a typical output signal from Honeywell 2793 IRCCD.

The timing patterns for the clocks were generated using a combination of stored PROM pattern and a binary counter scheme. Seven of the nine clocks were generated from a stored pattern read from a PROM. The remaining clocks were generated every alternate 32 cycles of the PROM clocks by using a preset binary counter and associated logic as shown in Fig. 7. In ad-

dition, a pixel-valid pulse (required for analog-to-digital conversion) was also generated in the PROM pattern.

A video preamplifier was provided inside the Dewar to drive the video signal cable. After appropriate dc level restoration, the video signal was digitized to 8 bits using the TRW TDC1007 flash analog-to-digital converter. The data were then stored in a dual-ported memory buffer using a direct memory access technique.

All the above CCD drive electronics and data acquisition circuits were located in close physical proximity to the interferometer and controlled by a local Intel 8088 microprocessor. A requirement of this particular instrument was that it should be controlled from a remote desktop computer (up to 25 m away). A serial data link was used for communication between the remote computer and the local 8088 microprocessor.

The 8088 microprocessor was also provided with an output port connected to a 12-bit digital-to-analog converter. This analog output voltage was then amplified to a high voltage for driving the piezoelectric transducer (PZT) used to move the reference mirror in the interferometer.

Figure 8 shows components of the data acquisition system.

The 8088 executed EPROM-resident firmware enabling it to perform the following tasks:

- (1) Move PZT to new position.
- (2) Take one frame of intensity data from CCD.
- (3) Transfer one frame of intensity data to remote computer.
- (4) Take four consecutive frames of intensity data moving the PZT to a new position between each frame.
- (5) Transfer all four intensity frames to remote computer.

Operations 1-3 could be used to obtain intensity data useful for system test and adjustment as well as for checking fringe visibility. Operations 4 and 5 were used for taking data for phase measurement. (The phase calculation was performed in the remote computer.)

In addition to the data acquisition system, an XYZ display was incorporated for display of real-time imagery from the IRCCD. This display proved essential for optical alignment and fringe location.

V. Direct Phase Measurement

Direct phase measurement interferometry was selected for use with the interferometer because it would provide good measurement accuracy and because it works well with CCD arrays.

Several techniques exist for direct phase measurement in interferometry.^{9,10} In a direct phase measurement interferometer, the phase of the reference beam is varied in a controlled manner. For some techniques the phase is changed in discrete steps while for other techniques the phase difference between the two interfering beams is changed at a constant rate with time. For the DF interferometer described in this paper, the phase of the reference beam is changed in discrete steps by use of a piezoelectric transducer that

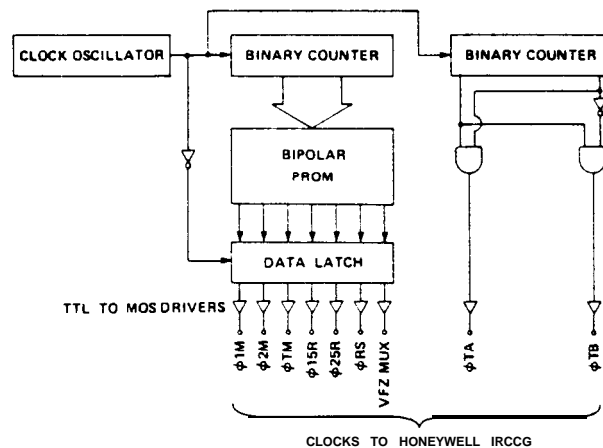


Fig. 7. Clock generation circuitry.

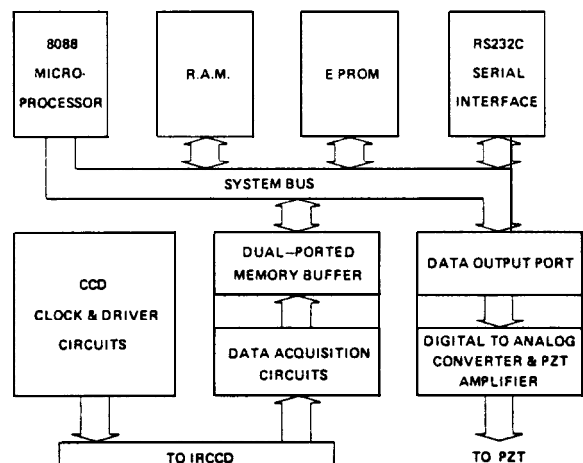


Fig. 8. Block diagram of data acquisition system.

moves the reference mirror (see Fig. 3). The detector array is read out four times, and between two consecutive measurements the reference mirror is moved approximately one-quarter of a wavelength.

The algorithm, which was described by Carré in 1966,¹¹ calculates the phase using four intensity readings. This can be seen as follows:

Equation (1) gives the irradiance that the detector would measure at the four phase steps. Between each readout of the detector, the phase of the reference beam is changed by an amount α .

$$\begin{aligned}
 A(x,y) &= I_1 + I_2 \cos[\phi(x,y)], \\
 B(x,y) &= I_1 + I_2 \cos[\phi(x,y) + \alpha], \\
 C(x,y) &= I_1 + I_2 \cos[\phi(x,y) + 2\alpha], \\
 D(x,y) &= I_1 + I_2 \cos[\phi(x,y) + 3\alpha].
 \end{aligned}
 \tag{1}$$

These four equations for the irradiance contain four unknowns: I_1 ; I_2 ; α ; and $\phi(x,y)$. $\phi(x,y)$ is the phase that we want to determine. If $\alpha = 90^\circ$,

$$\tan\phi(x,y) = \frac{D(x,y) - B(x,y)}{A(x,y) - C(x,y)}.
 \tag{2}$$

The real power of the above technique is that because of the subtraction process, fixed pattern noise across the detector is subtracted out, and because of the division process the gain in intensity variations across the detector drop out. These features are of particular importance in working with state-of-the-art IRCCD arrays.

By using Eq. (2), the wave front phase is measured modulo 2π . In reconstructing the wave front, the 2π discontinuities must be removed. A condition for removing the 2π discontinuities is that the phase difference between adjacent detector pixels must be $<\pi$. If this condition is satisfied and a phase difference of $>\pi$ is observed, an integer number of 2π values must be added or subtracted to eliminate the discontinuity in the measured wave front.

VI. Computer and Software

A Hewlett Packard 9836 desktop computer was used to control the taking of the data and the data analysis. The interferogram intensity was displayed on a color display. Software written in PASCAL does the phase calculations and removes 2π discontinuities in the phase wave front. The pupil is identified by making sure that either $A - C$ or $B - D$ in Eq. (2) is >3 bits of the 8 bits to which the signal is digitized. Points for which the differences are <3 bits are taken to be outside the pupil. The data are fit to nine Zernike polynomials, and any combination of tilt, focus, coma, astigmatism, and third-order spherical aberration can be removed from the data. A reference wave front can be subtracted from the data as the data are measured. This is very useful for removing known errors in the interferometer setup. Both 2-D color maps and 3-D wave front maps can be produced. All data can be stored on floppy disk for later analysis.

VII. Results and Conclusions

The output plots produced by the HP9836 are in color and do not reproduce well in black and white. For this reason we will not show intensity plots, and we will show only one 2-D phase map.

Figure 9 shows a 2-D phase map obtained using the interferometer. In this map approximately two waves of tilt are present across the wave front. The software can be used to subtract the tilt, and a result with tilt removed is shown in Fig. 10 as a 3-D view.

Satisfactory operation of the IRCCD was very dependent on critical adjustment of the voltage levels of certain clock and bias signals. However, once adjusted correctly, satisfactory device performance was obtained. A certain amount of electronic feedthrough noise and cross talk was present in the CCD drive electronics and data acquisition system, and this limited the SNR of the video signal.

One measure of system performance that can be easily performed is repeatability between successive phase measurements. The repeatability obtained during preliminary tests has been better than one-fiftieth of a wave rms for the wave front phase. A repeatability of one one-hundredth of a wave rms is often

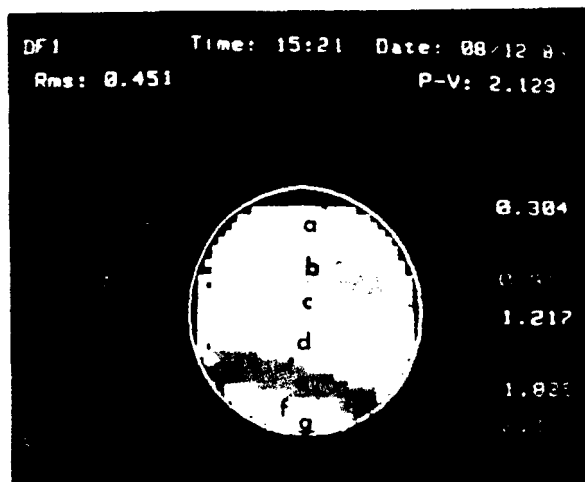


Fig. 9. Two-dimensional phase contour map before subtraction of tilt: (a) 0.304λ ; (b) 0.608λ ; (c) 0.913λ ; (d) 1.217λ ; (e) 1.521λ ; (f) 1.825λ ; (g) 2.129λ . Note that the letters on the contours do not appear on the actual contour map.

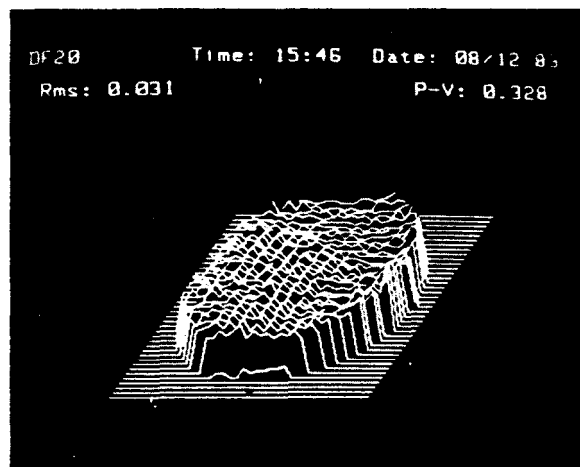


Fig. 10. Three-dimensional phase map after subtraction of tilt.

obtained. For these measurements we have had a path difference of <10 cm (to reduce effects of vibration and turbulence) and an array clocking speed of 250,000 pixels/sec.

As expected, direct phase measurement interferometry appears to work as well at $3.8\ \mu\text{m}$ as in the visible. While the DF laser is certainly not as convenient to use as a He-Ne or argon laser, the laser does give an acceptable output. Having to cool the IRCCD is an inconvenience but not a serious problem.

References

1. H. E. Bennett, "Large Optics Coating and Evaluation Facility Study," NWC TP 6177 (Aug. 1980).

2. R. E. Knowlden, "Wavefront Errors Produced by Multilayer Thin-Film Optical Coatings," Ph.D. Dissertation, U. Arizona (1981).
 3. T. Conklin and E. H. Stupp, "Applications of the Pyroelectric Vidicon," *Opt. Eng.* 15, 510 (1978).
 4. A. F. Milton, "Charge Transfer Devices for Infrared Imaging," in *Optical and Infrared Detectors*, R. J. Keyes, Ed. (Springer, New York, 1977), p. 197.
 5. J. J. Klein, N. L. Roberts, and G. D. Chin, "Infrared Camera System Developed to Use the Schottky-Barrier IRCCD Array," *RCA Eng.* 27, 3 (1982).
 6. C. L. Carrison and N. L. Foss, "Fixed Pattern Noise Compensation Techniques for Staring Infrared Focal Planes," *Opt. Eng.* 19, 5 (1980).
 7. E. L. Dereniak, R. A. Bredthauer, E. M. Hicks, J. E. Vicars, and R. A. Florence, "Microprocessor-Based Charge Coupled Device (CCD) Test Console," *Opt. Eng.* 21, 5 (1982).
 8. K. N. Prettyjohns, "Charge Coupled Device Image Acquisition for Digital Phase Measurement Interferometry," *Opt. Eng.* 23, 4 (1984).
 9. C. L. Koliopoulos, "Interferometric Optical Phase Measurement Techniques," Ph.D. Dissertation, Optical Sciences Center, U. Arizona (1981).
 10. J. C. Wyant and C. L. Koliopoulos, "Phase Measurement System for Adaptive Optics," *AGARD Conf. Proc.* 300 (1981).
 11. P. Carré, "Installation et Utilisation du Comparateur Photo-electrique et Interferential du Bureau International des Poids et Mesures," *Metrologia* 2, 13 (1966).
-